Multi-shaped cationic gold nanoparticle-L-cysteine-ZnSeS quantum dots hybrid nanozyme as an intrinsic peroxidase mimic for the rapid colorimetric detection of cocaine

Adegoke, Oluwasesan; McKenzie, Craig; Daeid, Niamh Nic

Published in:
Sensors and Actuators, B: Chemical

DOI:
10.1016/j.snb.2019.02.074

Publication date:
2019

Document Version
Peer reviewed version

Multi-shaped cationic gold nanoparticle-L-cysteine-ZnSeS quantum dots hybrid nanozyme as an intrinsic peroxidase mimic for the rapid colorimetric detection of cocaine

Oluwasesan Adegoke[a,*], Craig McKenzie[b], Niamh Nic Daeid[a,b]

[a]*Leverhulme Research Centre for Forensic Science, University of Dundee, Dundee, DD1 4GH*
[b]*Forensic Drug Research Group, Centre for Anatomy and Human Identification, School of Science and Engineering University of Dundee, Dundee, UK*

Author Accepted Manuscript version of Adegoke, O, McKenzie, C & Daeid, NN 2019, 'Multi-shaped cationic gold nanoparticle-L-cysteine-ZnSeS quantum dots hybrid nanozyme as an intrinsic peroxidase mimic for the rapid colorimetric detection of cocaine' Sensors and Actuators, B: Chemical, vol. 287, pp. 416-427. https://doi.org/10.1016/j.snb.2019.02.074

Abstract

Current presumptive tests for illicit drugs can suffer from false positive results and poor selectivity, and consequentially there is a need to develop new colour spot tests specifically designed to circumvent these existing challenges. In this work, we report on a new fluorescent hybrid nanozyme peroxidase-like catalytic colorimetric sensor and demonstrate proof of concept of this novel colorimetric-specific presumptive test for cocaine. A novel peroxidase-mimic hybrid nanozyme was developed based on the localized surface plasmon resonance-enhanced fluorescence interaction between multi-shaped cationic cetyltrimethylammonium bromide (CTAB)-functionalized gold nanoparticles (AuNPs) and anionic non-cadmium fluorescent-emitting L-cysteine-capped ZnSeS alloyed quantum dots (QDs). The affinity-based interaction of cocaine with the QDs-CTAB-AuNP surface was induced by its distinct structural conformation and this forms the basis for the selective recognition. Thus, the hybrid nanozyme could function both as a catalytic affinity-based receptor and as an optical signal transducer based on the catalysed oxidation of 3,5,5-tetramethylbenzidine by H_2O_2. A positive bluish-green colour, specific to cocaine recognition, was colorimetrically obtained under optimum catalytic conditions. The optimized assay system detected cocaine within two minutes with unique specificity and distinct colour reaction. Under the optimum cocaine reaction conditions, the analysis of other substances and drugs on the colorimetric response of the QDs-CTAB-AuNP hybrid nanozyme revealed no colour interference, thus demonstrating that the developed probe could be utilized as a presumptive colour spot test for cocaine.

KEYWORD: Nanozyme; peroxidase; colorimetric; plasmonic nanoparticle; quantum dots; cocaine detection

1. Introduction

Forensic laboratories are often called upon to identify tablets, liquids and unknown powders that may contain a controlled drug. In an increasingly complex illicit drug market, where a large number of new or novel psychoactive substances appear and disappear over time, the search for more robust methods for the detection, identification and quantification of analytes of forensic interest has placed a burden on forensic science providers to develop new analytical tools and methods to meet the demand **[1].** Presumptive tests **[2-5]** and confirmatory tests **[6-9]** are used by forensic drug chemists to analyse unknown substances and illicit drugs. In many cases, it is also common place for first responding law enforcement officers to determine whether or not a suspected substance contains an illicit drug (e.g. cocaine) using an 'off the shelf' presumptive test kit with confirmatory testing remaining the responsibility of the laboratory based forensic chemist. Colorimetric testing, involving the response of a specific reagent to a drug is the quickest method for drug detection and also the means to potentially unravel the drug class to which the substance belongs. Commercially available chemical spot test kits are intensively used by law enforcement agencies for the detection of drugs of abuse. However, even though many of these tests have been in existence for very many decades, their underpinning chemistry in some cases remains speculative or unknown and they are increasingly challenged in terms of specificity particularly as new drugs emerge onto the illicit market. For example, the Scott test commonly used for cocaine **[10,11]** gives false positive results for other substances **[12]**. Advances in sensitive and tuneable biosensor technology where nanoparticle chemistry is deployed to target specific small molecules is a potential pathway forward and this work concentrates on developing a proof of concept for this approach using cocaine as the target molecule.

After the discovery of iron oxide magnetic nanoparticles (Fe_3O_4 NPs) as a peroxidase mimic **[13,14]**, the term "nanozyme" was coined to describe nanomaterial-based artificial enzyme mimics **[15].** Since then, other metal oxide-based nanomaterials such as cerium oxide **[16]**, cobalt oxide **[17]**, manganese dioxide **[18]** and vanadium pentoxide **[19]** have also been reported as peroxidase mimics. In addition, metal-based nanomaterials such as plasmonic gold (Au) NPs **[20]**, platinum NPs **[21]**, and carbon-based nanomaterials also fulfil this function **[22,23].** Apart from the published reports on single and bi-metallic AuNP nanozymes, hybrid nanomaterials that combine the localized surface plasmon resonance (LSPR) properties of AuNPs and the quantum confinement properties of semiconductor quantum dot (QDs) nanocrystals have not previously been reported to be peroxidase mimics and their development as reported in this work could potentially pave the way for the construction of new generation hybrid nanozymes for biosensing applications.

In this work, we report for the first time on the development of a new hybrid fluorescent nanozyme biosensor exhibiting peroxidase mimicking activity for the colorimetric detection of cocaine. Electrostatic interaction between cationic cetyltrimethylammonium bromide (CTAB)-functionalized multi-shaped AuNPs and negatively charged, non-cadmium fluorescent emitting $_L$-cysteine ($_L$-cyst)-capped ZnSeS alloyed QDs was used to form the hybrid nanozyme. Upon binding, LSPR from CTAB-AuNPs induced fluorescence enhancement in the QDs, thus influencing the peroxidase mimicking activity of the hybrid nanozyme. The peroxidase mimic hybrid nanozyme sensor was used both as a catalytic receptor and as the signal transducer for cocaine identification, triggering a positive bluish-greenish colour for cocaine based on the catalysed oxidation of 3,3,5,5-tetramethylbenzidine (TMB) by H_2O_2. To the best of our knowledge, our work is the first to report on an affinity-based hybrid multi-shaped plasmonic NP-

QDs fluorescent nanozyme mimic as a colorimetric sensor for forensic analysis of drugs or indeed any other target molecule.

2. Experimental

2.1. Materials

Citric acid, TMB, ascorbic acid, nicotine, diltiazem (98%), levamisole HCl (99+%) and CTAB were purchased from Acros Organics. Silver nitrate ($AgNO_3$), sodium phosphate dibasic dodecahydrate, lidocaine hydrochloride (≥ 99 %), benzocaine (≥ 99 %), cocaine hydrochloride (≥ 97.5 %), sodium acetate, (+) methamphetamine hydrochloride, trioctylyphosphine oxide (TOPO), trioctylyphosphine (TOP), hexadecylamine (HDA), octadecene (ODE), selenium (Se), sulphur (S), oleic acid, phenacetin (≥ 98%) and H_2O_2 (30% w/w) in solution with stabilizer were purchased from Sigma Aldrich. Tris(hydroxymethyl)aminomethane was purchased from Formedium. Dimethyl sulfoxide (DMSO), tri-Sodium citrate dihydrate, diethylzinc (Et_2Zn) solution, myristic acid, $_L$-cyst, oleylamine (OLA) and gold (III) chloride trihydrate ($HAuCl_4.3H_2O$) were purchased from Thermo Fisher. Quinolin-8-yl 1-pentyfluoro-1H-indole-3-8-carboxylate (5F-PB-22), N-ethylpentylone hydrochloride, methylenedioxypyrovalerone hydrochloride (MDVP), benzylpiperazine dihydrochloride (BZP) and reference standards (all >98% pure) were synthesised, characterised and provided by Dr. Oliver B. Sutcliffe, Manchester Metropolitan University, UK. All other chemicals were used as received. The buffer solution used in this study was prepared in Milli-Q water.

2.2. Characterization

UV/vis absorption and fluorescence emission measurements were performed on a Cary Eclipse (Varian) spectrophotometer. Transmission electron microscopy (TEM) measurements were carried using a JEOL JEM-1200EX operated at 80 kV. Samples were deposited on a pioloform coated grid prior to imaging. The particle size distribution of the plasmonic NPs were analysed using ImageJ software. Energy dispersive X-ray (EDX) analysis was carried out using a JEOL JSM 7400F field emission scanning electron microscope integrated with an Oxford Instruments Inca EDX spectrometer. Powder X-ray Diffraction (XRD) analysis was carried out using a Siemens D5000 diffractometer with Cu Kα radiation ($\lambda = 1.54056$ nm) and data were obtained in the range of 3-60° using a 0.1° 2θ step size and a 3 s count time per step with a 0.066° slit width. FT-IR measurements were carried out using an Agilent Cary 630 FT-IR spectrometer. Absorbance measurements were recorded on a 800 TS microplate absorbance reader from BioTek.

2.3. Synthesis of multi-shaped CTAB-AuNPs

To synthesize CTAB-AuNPs **[24]**, growth solution containing a mixture of 10 mL 0.1 M CTAB, 5 mL 2.5 x 10^{-4} M $HAuCl_4.3H_2O$, 0.5 mL 0.004 M $AgNO_3$ and 0.4 mL 0.1 M ascorbic acid was stirred at room temperature. Thereafter, 100 µL of seed solution (5 mL 2.5 x 10^{-4} M $HAuCl_4.3H_2O$ + 10 mL 0.1 M CTAB + 0.6 mL 0.01 M $NaBH_4$) was added into the growth solution under stirring and the solution was left to stand for ~24 hours. The CTAB-stabilized AuNPs were purified by centrifugation, re-suspended in 50 mL of Milli-Q water and stored in the dark at room temperature.

2.4. Synthesis of L-cyst-ZnSeS alloyed QDs

Organic-phased non-cadmium emitting ZnSeS alloyed QDs were synthesized via the hot-injection organometallic synthetic route and a ligand exchange reaction was used to convert the hydrophobic nanocrystals to hydrophilic nanocrystals by replacing the organic-capped ligands with L-cyst thiol ligand. Under reflux, 5 mL Et_2Zn, 0.9 g TOPO, 1 mL TOP, 0.6 g HDA, 0.6 g myristic acid, 20 mL ODE, 2 mL OLA and 10 mL oleic acid were mixed in a 3-necked flask under N_2 gas flow for a few minutes (min). Thereafter, the solution was subjected to high temperature reaction to aid complexation of the Zn metal to the surfactants and organic ligand precursors. When the temperature reached ~320 $^{\circ}$C, 3 mL of TOPSe precursor (0.12 g Se + 5 mL TOP) was injected into the Zn reaction solution to aid the nucleation and growth of ZnSe core QDs. When the temperature of the solution reached ~330 $^{\circ}$C, TOPS precursor (0.16 g S + 0.9 g TOPO + 10 mL ODE, 1 mL TOP and 5 mL oleic acid) was injected to aid the nucleation and growth of alloyed ZnSeS QDs. A fraction of the ZnSeS alloyed QDs was injected out after ~35 min into a beaker, sealed with parafilm and kept in the dark for ~24 hours. Prior to ligand exchange reaction, the organic-phased QDs was dissolved in chloroform.

A ligand exchange reaction to replace the organic capping with water-soluble L-cyst thiol ligand was carried out by mixing the chloroform-dispersed QDs in a solution of 3 g KOH, 2.5 g L-cyst and 40 mL methanol. Appropriate volume of Millipore water was added into the solution to precipitate the hydrophilic QDs from the hydrophobic QDs and the solution was kept still for ~24 hours. The QDs were purified with acetone, chloroform/acetone/ethanol and acetone/ethanol mixture and thereafter dried in the fume hood. The surface capping with L-cyst ligand provided free carboxylate groups readily available for electrostatic interaction.

2.5. Assay procedure

All assay preparation and detection was carried out in a 96-well clear flat-bottom microplate. The QDs-CTAB-AuNP fluorescent hybrid nanozyme was formed via electrostatic interaction by mixing 3 mL of cationic CTAB-AuNPs (0.02 nM) with 3 mg/mL of L-cyst-capped ZnSeS QDs (1 mL). For quantitative cocaine detection, 20 µl of the hybrid nanozyme was mixed with 75 µl of cocaine (10–100 µM) in KCl-HCl buffer, pH 2.2, 45 µL TMB solution (0.003 M) and 30 µl H_2O_2 (1.2 M) solution. After adding TMB/H_2O_2 into the probe system, photographs of the colorimetric response were taken at ~2 min. The absorbance of the probe solution was recorded on a BioTek 800 TS microplate reader with a 630 nm filter after TMB/H_2O_2 addition.

3. Results and discussion

3.1. Structural properties

The surface morphology of the plasmonic cationic CTAB-AuNPs, L-cyst-capped ZnSeS QDs and the QDs-CTAB-AuNP hybrid nanozyme was analysed using TEM. Looking closely at the TEM micrograph of CTAB-AuNPs (Fig. 1A), a well-defined multi-shape mixture of spherical, cubic, bipyramidal, pentagonal and urchin particles was observed. The estimated average particle size was 58 nm. CTAB functioned as a stabilizer while ascorbic acid acted as a reducing agent for the Au ion in which higher reduction rates and the strong effect of Ag precursor led to the formation of the multi-shaped surface morphology **[25].** The surface morphology of the L-cyst-capped ZnSeS QDs (Fig 1B) and the hybrid nanozyme (Fig. 1C) was heterogenous in nature as evident from the polydisperse particle morphology. Zn-based non-cadmium emitting QDs are known to exhibit lesser optical properties than the well-known Cd-based QDs **[26]**. However, to avoid the inherent toxicity of Cd-based QDs, Zn-based QDs was the choice of nanocrystal in this work.

PXRD was used to study the crystal nature of the colloidal L-cyst-capped ZnSeS QDs, CTAB-AuNPs and the QDs-CTAB-AuNP hybrid nanozyme. To confirm the formation of the alloyed ZnSeS QDs, we compared the diffraction pattern of ZnSe core and the alloyed ZnSeS QDs (Fig. 2A). From the diffraction pattern, a slight shift to higher Bragg angle was observed for the alloyed ZnSeS QDs relative to the ZnSe core. The shift was clearly visible in the diffraction peak at the {220} and {311} plane, thus depicting structural changes in the alloyed ZnSeS QDs relative to the ZnSe core. The diffraction pattern can also be attributed to the zinc-blende crystal structure due to the formation of the three prominent peaks at planes {111}, {220} and {311} respectively **[27]** and can be assigned to the JCPDS Card No.19-0191. For the diffraction pattern of CTAB-AuNPs shown in Fig. 2B, the position of the peaks and the assigned plane at {111}, {112}, {211}, {220}, {310} and {200} is indicative of cubic crystal structure **[28].** The analysis of the diffraction pattern of the QDs-CTAB-AuNP hybrid nanozyme (Fig 2C), reveal the presence of the prominent QDs peak at the {111} plane while the less prominent peaks at the {220} and {311} plane were weakly projected. This suggest that the electrostatic interaction between the L-cyst-capped ZnSeS QDs and CTAB-AuNPs induced the structural change in the diffraction pattern of the QDs-CTAB-AuNP hybrid nanozyme.

The elemental analysis of L-cyst-ZnSeS QDs was qualitatively and quantitatively assessed by EDX spectroscopy. As shown in Fig. S1, the qualitative Zn, Se, S metal components of the alloyed QDs were strongly detected. In addition, C and O present in the functional moiety of the L-cyst thiol capping ligand was also identified. The elemental compositions are: Zn (34.15%), Se (6.26%), S (22.45%), C (26.63%) and O (10.50%), thus suggesting that the QD nanocrystal is rich in Zn.

3.2. Optical properties

3.2.1. UV/vis and fluorescence emission spectra

The optical properties of AuNPs occur primarily due to their distinctive SPR absorption property. Alteration of the local electron confinement which is reflected via changes in the SPR absorption band and via the colour of the colloidal solution is induced by alteration/change in the plasmonic NP geometry, shape or size **[29].** Changes in the colour of the colloidal solution and the SPR absorption peak also forms the basis for colorimetric plasmonic sensors and is reflected by either analyte-induced NP aggregation or disaggregation of the particles**.** In addition, colorimetric probes based on changes in the surrounding dielectric constant of plasmonic NPs by target analytes also alters the SPR absorption peak **[29].** Fig. 3A shows the SPR absorption peak of the cationic CTAB-AuNPs. The strong plasmon absorption at around 564 nm is distinctive of non-spherical particles [**30]** while the absence of broadening in the SPR absorption peak provides direct evidence for the stability and unagglomerated state of the cationic plasmonic CTAB-AuNP. For the QDs (Fig. 3B), the broad excitonic absorption spectrum is indicative of a heterogenous growth pattern and a polydisperse particle morphology **[31],** described earlier in the TEM image.

Fig 3B shows the fluorescence emission spectrum of the QDs with a wavelength maximum at 525 nm (λ_{exc} = 200 nm). The fluorescence quantum yield which is a measure for assessing the surface quality of the QDs was determined according to Eq. 1:

$$\Phi_F^{QD} = \Phi_F^{R6G} \frac{F_{QDs} \cdot OD_{R6G(\lambda exc)} \cdot n^2_{water}}{F_{R6G} \cdot OD_{QD(\lambda exc)} \cdot n^2_{ethanol}} \quad (1)$$

Φ_F^{R6G} is the fluorescence quantum yield of the reference standard, rhodamine 6G in ethanol (Φ = 0.95)) **[32]**, F_{QDs} and F_{R6G} are the sum of the integrated fluorescence intensity of the QDs and

standard, $OD_{R6G(\lambda exc)}$ and $OD_{QD_{(\lambda exc)}}$ are the optical densities of the standard and QDs while ${n^2}_{water}$ and $n^2_{ethanol}$ are the square of the refractive indices of the solvents used to dissolve the QDs and standard respectively. The calculated fluorescence quantum yield of the QDs was 52%. The relatively high quantum yield value provides strong evidence for the moderate suppression of surface defect states that act as dangling bonds to induce a non-radiative exciton recombination state in the QDs.

3.2.2. LSPR-enhanced fluorescence of L-cyst-ZnSeS QDs

The chemistry underpinning the effects of noble metal plasmonic NPs on the fluorescence of light-emitting fluorophores have long been researched and is well documented in the literature **[33,34]**. Metal plasmonic NPs are known to act as either radiative fluorescence quenchers or radiative fluorescence enhancers based on strong dependence on their shape, size, and distance between the fluorophore and plasmonic NP in a donor-acceptor relationship **[35,36]**. The competition between fluorescence quenching and enhancement, relates to the dielectric dispersion of the materials and the electric field magnitude at the particle surface which results in plasmon-induced fluorescence quenching from small-sized plasmonic NPs or plasmon-induced fluorescence enhancement from larger-sized plasmonic NPs **[34,36].** Lakowicz used the radiating plasmon model to demonstrate that depending on the coupling nature between the oscillating SPR of the metal NP and the fluorophore in close distance to the metal surface, the plasmon-induced radiative fluorescence quenching of the fluorophore is dominated by the absorption cross section of the NP while the plasmon-induced radiative fluorescence enhancement is dominated by the scattering cross section of the NP.

Fig. 3C shows the spectral overlap between the LSPR absorption band of CTAB-AuNPs and the fluorescence emission spectrum of L-cyst-ZnSeS QDs. The strong overlap, which reveals close proximity of the QDs PL spectrum to the LSPR absorption band of the NP, can be attributed to the combination of the NP shape and size and the PL spectral emission of the QDs. Comparison of the PL emission spectra of the unbonded QDs and the hybrid CTAB-AuNPs-QDs (Fig. 3D), reveals a marked enhancement in fluorescence intensity for the latter. Due to the LSPR-induced fluorescent enhancement of the QDs, the radiating plasmon model proposed by Lakowicz suggests that the scattering cross section of the NP dominates over the absorption cross section. Hence, CTAB-AuNPs acts as a donor of plasmon energy while L-cyst-ZnSeS QDs acts as an acceptor. It has been reported that plasmonic NPs with size less than 40 nm are strong radiative fluorescence quenchers while NPs with size > 40 nm are strong radiative fluorescence enhancers **[37].** Therefore, the LSPR-induced fluorescence enhancement of L-cyst-ZnSeS QDs by the 58 nm-sized CTAB-AuNPs as observed in this work, corroborates the underpinning chemistry of published plasmon-enhanced fluorescence of fluorophores.

3.2.3. FT-IR analysis

FT-IR analysis was used to probe the electrostatic interaction between CTAB-AuNPs and the L-cyst-ZnSeS QDs. From Fig. 3E, L-cyst-ZnSeS QDs is characterized by the asymmetric and symmetric -COO^- stretching band at 1576 cm^{-1} and 1388 cm^{-1} while the band at 3365 cm^{-1} is assigned to the -N-H stretch. For CTAB-AuNPs, the bands at 2915 cm^{-1} and 2847 cm^{-1} is assigned to the -C-H stretch while the bands at 1464 cm^{-1} is assigned to the -C-H bend. For the QDs-CTAB-AuNP hybrid nanozyme, the band at 1617 cm^{-1} which is absent in CTAB-AuNPs and the L-cyst-ZnSeS QDs can be used as a proof of the electrostatic interaction **[38]**. In addition, the -C-H

bending and stretching band at 1460 cm^{-1} and 2913 cm^{-1} for the QDs-CTAB-AuNP hybrid nanozyme are shifted to lower wavenumbers relative to CTAB-AuNPs, thus tentatively confirming the established electrostatic interaction.

3.3. Catalytic activity

The efficiency of the peroxidase-like catalytic activity of the QDs-CTAB-AuNP hybrid nanozyme sensor to recognize cocaine was investigated. From Fig 4A and 4B, the mixture of TMB/H_2O_2 was colourless and exhibited no absorption peak while the mixture of the QDs-CTAB-AuNP hybrid nanozyme and TMB/H_2O_2 (without cocaine) showed no colour and absorption peak unique to a peroxidase catalytic activity. However, a strong catalytic colorimetric response and corresponding characteristic absorption at ~655 nm, unique to the characteristic peroxidase catalytic activity was exhibited when cocaine solution (100 µM) was added to the QDs-CTAB-AuNP hybrid nanozyme and TMB/H_2O_2 mixture.

Scheme 1 shows the descriptive working principle of the QDs-CTAB-AuNP hybrid nanozyme peroxidase-like catalytic cocaine biosensor. Due to the electrostatic interaction between cationic CTAB-AuNPs and anionic $_L$-cyst-capped ZnSeS, LSPR from the plasmonic NP induced fluorescence intensity enhancement signal in the QDs (Fig. 3B). Such LSPR-mediated fluorescence interaction has been reported for several biosensors **[39,40]**. The widely reported mechanism of nanozyme-based peroxidase-like biosensors is the catalysation of H_2O_2 into hydroxyl radicals ($^{\cdot}OH$) by a nanozyme catalyst in the presence of a suitable substrate **[41]**. To understand the interaction between the QDs-CTAB-AuNP hybrid nanozyme and cocaine, we undertook direct fluorescence measurements as shown in Fig. S2. It was observed that the direct addition of cocaine to the hybrid nanozyme triggered further fluorescence enhancement which

could be explained in terms of affinity-based interaction between the QDs-CTAB-AuNP hybrid nanozyme and cocaine. Within the aqueous hybrid environment, hydrophobic molecules can be trapped by CTAB and adsorbed onto the AuNP surface, thus aiding strong interaction with an affinity-based analyte (cocaine in this case) and leading to the enhanced fluorescence intensity of the QDs. Such interaction has been reported for surface-enhanced Raman scattering, surface-enhanced fluorescence and hydrophobic molecule-based photochemical reactions **[42].** From a fluorescence theoretical perspective for semiconductor QDs, the enhanced fluorescence intensity observed for the QDs-CTAB-AuNP hybrid nanozyme from the cocaine interaction, implies that the electron-hole exciton pair of the QDs recombined and promoted an electron from the valence band to the conduction band. This led to the creation of positive holes in the valence band and excited electrons in the conduction band **[43,44].** Thus, the QDs-CTAB-AuNP fluorescence hybrid nanozyme has the potential to decompose H_2O_2 to ·OH and oxidize the chromogenic substrate substrate TMB to yield a bluish-green colour for cocaine identification.

3.4. Effect of buffer type

During enzymatic assays, buffers serve to stabilize and adjust the desired pH. Besides selecting the appropriate pH required, the nature of the buffer components, concentration and the ionic strength all play important roles for optimum catalytic reaction. The effect of buffer type was investigated to probe the efficiency of the detection medium to aid the peroxidase-like catalytic activity of the QDs-CTAB-AuNP hybrid nanozyme for cocaine colorimetric recognition. Cocaine HCl (100 µM) was prepared in citrate-phosphate, pH 4.0 and KCl-HCl, pH 2.2 buffer due to reported stability of cocaine HCl in these buffers **[45]**. Borax-HCl, pH 8.0 was also chosen for further investigation as cocaine is known to hydrolyze to benzoylecgonine at pH > 5.5 **[46]**.

Sodium citrate, pH 4.2 buffer was chosen due to its use as a detection medium for plasmonic NPs in peroxidase-mimic reaction **[47]**. Fig. 5 shows the catalytic response of the QDs-CTAB-AuNP hybrid nanozyme to cocaine using the four different buffer types. It was evident that no catalytic activity was observed by the QDs-CTAB-AuNP hybrid nanozyme when citrate-phosphate pH 4.0, sodium citrate pH 4.2 and borax-HCl pH 8.0 buffers were used. However, high catalytic activity accompanied by a bluish-green colorimetric response was exhibited by the QDs-CTAB-AuNP hybrid nanozyme biosensor when KCl-HCl pH 2.2 buffer was used. It was also noteworthy that within 2 minutes (min), cocaine was detected visually with high catalytic activity under optimum conditions. Since the nature and ionic strength of buffers play important roles in enzyme activity as well as the stability of cocaine, components of the buffer such as mono- or di-valent metal ions directly influence the catalytic activity of the enzyme. Therefore, the catalytic-induced reaction of the hybrid nanozyme for cocaine recognition in 0.1 M KCl-HCl, pH 2.2 buffer may be explained in terms of the stabilizing effects of the buffer components for cocaine and was the reason why this buffer was chosen for the colorimetric assay. The effects of pH on the catalytic activity of the QDs-CTAB-AuNP hybrid nanozyme for cocaine detection is discussed in the Supplementary Information.

3.5. Elucidation of the affinity-based cocaine interaction

Understanding the structure and conformation of molecules is crucial in the context of unravelling how drugs interact with the hydrophobic and hydrophilic surfaces of materials. It is imperative to note that the high affinity-based binding of cocaine to the QDs-CTAB-AuNPs hybrid surface is quite intriguing. Thus, to unravel the mystery behind the strong selectivity reaction of cocaine, we have displayed the structure of cocaine and the other tested drug substances and drugs in Scheme

2. We believe a possible mode of interaction of the catalytic sensor to cocaine can be unravelled by elucidating the structural conformation of cocaine in comparison to the non-selective compounds. Observing closely the molecular structure of cocaine, it is apparent that cocaine possesses a unique carbomethoxy and benzoyl group accompanied by a tropane alkaloid ring that is absent in the other compounds. Stojanovic et al., has previously used the lack of enantio-differentiation in the binding affinity of cocaine to suggest that enantiomers of cocaine exhibit similar fluorescence quenching abilities and are indistinguishable in their binding interactions **[48]**. Hence, we can infer from Stojanovic's theoretical description of cocaine binding, that the benzoyl group of cocaine and the planes of symmetry of the tropane ring can be aligned with the plane of the receptor molecule ($_{L}$-cyst-ZnSeS QDs-CTAB-AuNPs in this case), such that the carbomethoxy group of cocaine projects away from the lipophilic cavity.

The constraints afforded by intramolecular hydrogen bonding is known to influence the properties of molecules. The intramolecular hydrogen bond between the carbomethoxy group and the tropane ring has been proposed by Johnston et al., to induce stability in cocaine such that it inhibits the rotation of the carbomethoxy group and prevents cocaine from folding back on itself ensuring that the benzene ring tilts at an angle of 30 °C, preventing it from orientating itself towards the tropane ring **[49].** Since intramolecular hydrogen bonding is also known to be strongly associated with water, we believe the ability of cocaine to strongly bind water to the atoms within its non-covalent bond, coupled with the aforementioned intramolecular hydrogen bonding between the carbomethoxy group and the tropane ring, a strong affinity to the QDs-CTAB-AuNP hybrid surface is created. Such a mode of interaction has been reported previously for the movement of cocaine across the blood-brain barrier **[48]**. This demonstrates that the distinct structural conformation of cocaine plays a major role in the binding affinity to the hybrid nanozyme surface.

3.6. Effects of TMB and H_2O_2

The effects of TMB substrate and H_2O_2 oxidant on the peroxidase-like catalytic activity of the QDs-CTAB-AuNP hybrid nanozyme for cocaine recognition was investigated. Fig 6A shows the catalytic response of the hybrid nanozyme to cocaine at different TMB concentrations. A systematic increase in catalytic activity proportionate to the increase in TMB concentration was observed. In contrast, the catalytic response of the hybrid nanozyme to cocaine as a function of increasing H_2O_2 concentration did not follow any definite trend (Fig. 6B). Further studies were undertaken to understand the catalytic activity of TMB and H_2O_2 as a function of time. As revealed in Fig. 6C and D, a direct linear relationship was observed in the catalytic response of each TMB and H_2O_2 concentration as a function of time. Specifically, the linear reaction rate increased with TMB and H_2O_2 concentration but was more pronounced in quantitative signal for TMB than for H_2O_2. Hence, we chose 3000 µM TMB and 1.2 M H_2O_2 concentration as the optimum concentration for substrate and oxidant respectively.

3.7. Selectivity to cocaine

The catalytic efficiency of the QDs-CTAB-AuNP hybrid nanozyme biosensor for cocaine was also investigated in comparison with a selection of other substances. L-nicotine (a potent parasympathomimetic stimulant used in cigarettes), *N*-ethylpentylone (N-EP; a stimulant drug of the synthetic cathinone class), 5F-PB-22 (1-(5-fluoropentyl)-8-quinolinyl ester-1H-indole-3-carboxylic acid; a synthetic cannabinoid receptor agonist), benzocaine (an anaesthetic and adulterant often found in cocaine in the UK), BZP (Benzylpiperazine; a recreational drug of the piperazine class), MDVP (Methylenedioxypyrovalerone; a stimulant drug of the synthetic cathinone class), methamphetamine (an amphetamine-type stimulant), lidocaine (an anaesthetic

and adulterant commonly found in cocaine in some jurisdictions), phenacetin (a pain-relieving dug and adulterant commonly found in cocaine in some jurisdictions) **[50]**, levamisole (a medication drug used to treat parasitic worm and adulterant commonly found in cocaine in some jurisdictions) **[51]** and diltiazem (used in hypertension treatment and adulterant commonly found in cocaine in some jurisdictions) **[52]** were tested for their ability to trigger a colour change (false positive) based on the peroxidase-like catalytic activity of the QDs-CTAB-AuNP hybrid nanozyme for cocaine. As shown in Fig. 7, no catalytic response from any of the other tested substances was observed in comparison to the strong catalytic response and bluish-green colour observed for cocaine. Under the optimum catalytic reaction conditions used to detect cocaine, no colorimetric response was observed for any of the other substances tested. Therefore, it is reasonable to suggest that the developed QDs-CTAB-AuNP hybrid nanozyme biosensor could be used as a presumptive colour spot test for cocaine.

3.8. Quantitative cocaine detection

Quantitative detection of cocaine in the concentration range of 10 to 100 µM was carried out using the peroxidase-like catalytic QDs-CTAB-AuNP hybrid nanozyme biosensor. Fig. 8A shows the quantitative colorimetric response to cocaine after 2 min while the corresponding catalytic response is shown in Fig. 8B. A steady enhancement in catalytic signal which linearly correlated to the concentration of cocaine revealed the quantitative efficiency of the QDs-CTAB-AuNP hybrid nanozyme biosensor. The limit of detection (LOD) was calculated by multiplying the standard deviation of blank measurements (n = 8 (0.000463)) by 3 and dividing by the slope of the linear calibration curve (0.0108) (inset of Fig. 8B). The LOD obtained for cocaine detection was 128 nM (43.5 ng/mL cocaine base) for the QD-57 nm-CTAB-AuNPs hybrid nanozyme.

Since the optical properties of NPs are known to be dependent on their size, it is reasonable to suggest that the sensitivity of the catalytic assay can be tuned according to the plasmonic NP size. Hence, we investigated the effect of the plasmonic CTAB-AuNPs size and the effect of citrate-AuNPs on the sensitivity of the cocaine catalytic assay. Fig. S4 shows the colorimetric and catalytic response of the 37 nm and 39 nm-sized CTAB-AuNPs-QD hybrid nanozyme to cocaine detection. A strong catalytic response to cocaine was observed with minimal signal difference for the different-sized CTAB-AuNP-bonded QDs, while a very weak catalytic signal was observed for citrate-AuNPs. In general, the LOD of the cocaine peroxidase-mimic assay using the different-sized CTAB-AuNPs followed the order QD-37 nm CTAB-AuNPs (112 nM (38.1 ng/mL)) > QD-58 nm CTAB-AuNPs (128 nM (43.5 ng/mL)) > QD-39 nm CTAB-AuNPs (135 nM (45.9 ng/mL)). Comparison of the analytical performance of the QDs-CTAB-AuNP hybrid nanozyme biosensor with other colorimetric biosensors for cocaine demonstrated a considerable improvement in either the detection time or sensitivity, or both, compared to previously reported probes (Table 1).

3.9. Comparative effects of sensitivity and selectivity

Under similar experimental conditions, the catalytic sensitivity and specificity of the QDs-CTAB-AuNP hybrid nanozyme to cocaine was compared with the QDs alone, CTAB-AuNPs and citrate-AuNPs (a known nanozyme) **[47]**. As shown in Fig. S5, no catalytic response was observed for the QDs alone while a weak catalytic response was observed for citrate-AuNPs and a strong catalytic response, higher than that exhibited by the hybrid nanozyme was observed for CTAB-AuNPs. However, probing the colorimetric selectivity of the QDs-CTAB-AuNP hybrid nanozyme to cocaine in comparison to citrate-AuNPs and CTAB-AuNPs, we observed poor selectivity for cocaine when CTAB-AuNPs and citrate-AuNPs were used. Fig. S6 shows the comparative time

course colorimetric response of the QDs-CTAB-AuNP hybrid nanozyme, citrate-AuNPs and CTAB-AuNPs to cocaine, methamphetamine and lidocaine. From the time course results, no colour reaction was observed for methamphetamine and lidocaine when using QDs-CTAB-AuNP hybrid nanozyme as the catalyst probe, but significant colorimetric interference was observed for CTAB-AuNPs. Both methamphetamine and lidocaine displayed a blue colour reaction to cocaine using CTAB-AuNPs nanozyme with the intensity of the colour being higher for lidocaine than for methamphetamine. In addition to the lower catalytic activity exhibited by citrate-AuNPs nanozyme to cocaine in comparison to the hybrid nanozyme, lidocaine displayed a less intense blue colour with time as shown in Fig. S6B. Thus, it is reasonable to conclude that the QDs-CTAB-AuNP hybrid nanozyme is a suitable catalyst probe for cocaine colorimetric recognition based on its superior selectivity.

3.10. Detection of cocaine in mixed drug samples

The catalytic efficiency of the CTAB-AuNP-QDs hybrid nanozyme to detect cocaine in mixed drug samples was investigated. Phenacetin, diltiazem and levamisole, all known adulterants previously detected in cocaine were chosen and different concentrations of cocaine (100, 75 and 50 μM) were added into an assay solution containing a fixed concentration of the adulterant (100 μM). Table 2 shows the analytical performance of the CTAB-AuNP-QDs hybrid nanozyme to cocaine detection in mixed drug samples while Fig. S7 shows the corresponding colorimetric response. From the data, we found that our peroxidase-like catalytic sensor can colorimetrically recognise cocaine in the tested mixed samples. Particularly, we found that the recovery of cocaine increased as the concentration of cocaine decreased in the mixed sample solution. Hence, it is

reasonable to conclude that the hybrid peroxidase-like catalytic sensor developed in this work is suitable to detect cocaine in adulterated drug samples.

4. Conclusions

The electrostatic interaction between cationic multi-shaped CTAB-AuNPs and anionic $_{L}$-cyst-ZnSeS QDs has revealed a new LSPR-enhanced hybrid artificial nanozyme mimicking the peroxidase-like catalytic activity of natural enzymes. Under optimum conditions, we found cocaine to exhibit high affinity for the hybrid nanozyme based on strong affinity to the QDs-CTAB-AuNP's surface. With the use of the new hybrid nanozyme sensor as a catalytic receptor and as a signal transducer, we have developed a rapid and selective colorimetric sensor for cocaine based on a TMB catalysed H_2O_2 system. A positive bluish-green colour was colorimetrically transduced within 2 min for cocaine with no colour interference observed from other tested substances and drugs under the optimum reaction conditions. This provides a convincing proof of concept application for the developed biosensor within the domain of forensic drug analysis.

Acknowledgements

We gratefully acknowledge the support of the Leverhulme Trust for funding this work.

Appendix A. Supporting information

Supplementary data associated with this article can be found in the online version at doi:

References

[1] J. Gooch, B. Daniel, M. Parkin, N. Frascione, Developing aptasensors for forensic analysis, Trac-Trend Anal. Chem. 94 (2017) 150-160.

[2] C. Anderson, Presumptive and confirmatory drug tests, J. Chem. Edu. 82 (2005) 1809-1810.

[3] A. Choodum, N. Nic Daeid, Rapid and semi-quantitative presumptive tests for opiate drugs, Talanta 86 (2011) 284– 292.

[4] M. Philip, S. Fu, A review of chemical 'spot' tests: A presumptive illicit drug identification technique, Drug Test Anal. 10 (2018) 95-108.

[5] M. Philp, R. Shimmon, M. Tahtouh, S. Fu, Development and validation of a presumptive color spot test method for the detection of synthetic cathinones in seized illicit materials, Forensic Chem. 1 (2016) 39–50.

[6] A.S. Dias, A.L. Castro, P. Melo, S. Tarelho, P. Dominques, J.M. Franco, A fast method for GHB-GLUC quantitation in whole blood by GC–MS/MS (TQD) for forensic purposes, J. Pharmaceut. Biomed. 150 (2018) 107–111.

[7] S. Mizuno, X-P. Lee, M. Fujishiro, T. Matsuyama, M. Yamada, Y. Sakamoto, M. Kusano, K. Zaitsu, C. Hasegawa, I. Hasegawa, T. Kumazawa, A. Ishii, K. Sato, High-throughput determination of valproate in human samples by modified QuEChERS extraction and GC-MS/MS, Legal Med. 31 (2018) 66–73.

[8] B. Moslah, M. Araoud, M.A. Nouioui, S. Najjar, D. Amira, N. Ben Salah, A. Hedhili, Fast screening tests for the simultaneous detection of 11 drugs of abuse in urine specimens. A forensic epidemiology study of 28,298 cases in Tunisia, Forensic Sci. Int. 283 (2018) 35–40.

[9] A. Orfanidis, O. Mastrogianni, A. Koukou, G. Psarros, H. Gika, G. Theodoridis, N. Raikos, A GC–MS method for the detection and quantitation of ten major drugs of abuse in human hair samples, J. Chromatogr. B, 1047 (2017) 141–150.

[10] J. Fasanello, P. Higgins, Modified Scott test for cocaine base or cocaine hydrochloride, Microgram 19 (1986) 137– 138.

[11] L.J. Scott Jr., Specific field test for cocaine, Microgram 6 (1973) 179–181.

[12] Y. Tsumura, T. Mitome, S. Kimoto, False positives and false negatives with a cocaine-specific field test and modification of test protocol to reduce false decision, Forensic Sci. Int. 155 (2005) 158–164.

[13] L.Z. Gao, J. Zhuang, L. Nie, J.B. Zhang, Y. Zhang, N. Gu, T.H. Wang, J. Feng, D.L. Yang, S. Perrett, X. Yan, Intrinsic peroxidase-like activity of ferromagnetic nanoparticles, Nat. Nanotechnol. 2 (2007) 577-583.

[14] H. Wei, E. Wang, Fe_3O_4 Magnetic nanoparticles as peroxidase mimetics and their applications in H_2O_2 and glucose detection, Anal. Chem. 80 (2008) 2250-2254.

[15] H. Wei, E. Wang, Nanomaterials with enzyme-like characteristics (nanozymes): next-generation artificial enzymes, Chem. Soc. Rev. 42 (2013) 6060-6093.

[16] J. S. Mu, Y. Wang, M. Zhao and L. Zhang, Intrinsic peroxidase-like activity and catalase-like activity of Co_3O_4 nanoparticles, Chem. Commun. 48 (2012) 2540–2542.

[17] W. Chen, J. Chen, A.L. Liu, L.M. Wang, G.W. Li, X.H. Lin, Peroxidase- like activity of cupric oxide nanoparticle, ChemCatChem. 3, (2011) 1151–1154.

[18] Y. Wan, P. Qi, D. Zhang, J.J. Wu, Y. Wang, Manganese oxide nanowire-mediated enzyme-linked immunosorbent assay, Biosens. Bioelectron. 33 (2012) 69–74.

[19] R. Andre, F. Natalio, M. Humanes, J. Leppin, K. Heinze, R. Wever, H.C. Schroder, W.E. G. Muller, W. Tremel, V_2O_5 Nanowires with an Intrinsic Peroxidase- Like Activity, Adv. Funct. Mater. 21 (2011) 501–509.

[20] Y. Jv, B. X. Li, R. Cao, Positively-charged gold nanoparticles as peroxidiase mimic and their application in hydrogen peroxide and glucose detection, Chem. Commun. 46 (2010) 8017–8019.

[21] L. B. Zhang, L. Laug, W. Munchgesang, E. Pippel, U. Gosele, M. Brandsch and M. Knez, Nano Lett., 2010, 10, 219–223.

[22] M. Liu, H. M. Zhao, S. Chen, H. T. Yu, X. Quan, Interface engineering catalytic graphene for smart colorimetric biosensing, ACS Nano 6 (2012) 3142–3151.

[23] Y. P. Ye, T. Kong, X. F. Yu, Y. K. Wu, K. Zhang and X. P. Wang, Enhanced nonenzymatic hydrogen peroxide sensing with reduced graphene oxide/ferroferric oxide nanocomposites, Talanta, 89 (2012) 417–421.

[24] H.M. Hen, R.-S. Liu, D.P. Tsai, A versatile route to the controlled synthesis of gold nanostructures, Cryst. Growth Des. 9 (2009) 2079-2087.

[25] C.J. Ward, R. Tronndorf, A.S. Eustes, M.L. Auad, E.W. Davis, Seed-mediated growth of gold nanorods: limits of length to diameter ratio control, (2014), Article ID 765618.

[26] R. Gill, M. Zayats, I. Willner, Semiconductor quantum dots for bioanalysis, Angew. Chem. Int. Ed. 47 (2008) 7602–7625.

[27] O. Adegoke, K. Takemura, E.Y. Park, Plasmonic oleylamine-capped gold and silver nanoparticle-assisted synthesis of luminescent alloyed CdZnSeS quantum dots, ACS Omega 3 (2018) 1357−1366.

[28] G.R. Kumar, A.D. Savariraj, S.N. Karthick, S. Selvam, B. Balamuralitharan, H.-J. Kim, K. K. Viswanathan, M. Vijaykumar, K. Prabakar, Phase transition kinetics and surface binding states of methylammonium lead iodide perovskite, Phys. Chem. Chem. Phys. 18 (2016) 7284—7292.

[29] E. Priyadarshini, N. Pradhan, Gold nanoparticles as efficient sensors in colorimetric detection oftoxic metal ions: A review, Sensor. Actuat. B 238 (2017) 888–902.

[30] S. Kundu, L. Peng, H. Liang, A new route to obtain high-yield multiple-shaped gold nanoparticles in aqueous solution using microwave irradiation, Inorg. Chem. 47 (2008) 6344-6352.

[31] O.S. Oluwafemi, N. Revaprasadu, O.O. Adeyemi, A facile “green” synthesis of ascorbic acid-capped ZnSe nanoparticles, Colloid Surface B 79 (2010) 126–130.

[32] L. Qu, X. Peng, Control of photoluminescence properties of CdSe nanocrystals in growth, J. Am. Chem. Soc. 124 (2002) 2049-2055.

[33] K.H. Drexhage, Influence of a dielectric interface on fluorescence decay time, J. Luminesc. 1.2 (1970) 693–701.

[34] J.R. Lakowicz, Radiative decay engineering 5: metal-enhanced fluorescence and plasmon emission, Anal. Biochem. 337 (2005) 171-194.

[35] T.L. Jennings, M.P. Singh, G.F. Strouse, Fluorescent lifetime quenching near d = 1.5 nm gold nanoparticles: probing NSET validity, J. Am. Chem. Soc. 128 (2006) 5462–5467.

[36] T. Pons, I.L. Medintz, K.E. Sapsford, S. Higashiya, A.F. Grimes, D.S. English, H. Mattoussi, On the quenching of semiconductor quantum dot photoluminescence by proximal gold nanoparticles, Nano Lett. 7 (2007) 3157–3164.

[37] T. Jennings, G. Strouse, Past, present, and future of gold nanoparticles, AdV. Exp. Med. Biol. 2007, 620, 34–47.

[38] B. Baruah, C. Craighead, C. Abolarin, One-phase synthesis of surface modified gold nanoparticles and generation of SERS substrate by seed growth method, Langmuir 28 (2012) 15168−15176.

[39] O. Adegoke, M. Morita, T. Kato, M. Ito, T. Suzuki, E.Y. Park, Localized surface plasmon resonance-mediated fluorescence signals in plasmonic nanoparticle-quantum dot hybrids for ultrasensitive Zika virus RNA detection via hairpin hybridization assays, Biosens. Bioelectron. 94 (2017) 513-522.

[40] F. Nasrin, A.D. Chowdhury, K. Takemura, J. Lee, O. Adegoke, V.P. Deo, F. Abe, T., Suzuki, E.Y. Park, Single-step detection of norovirus tuning localized surface plasmon resonance-induced optical signal between gold nanoparticles and quantum dots, Biosens. Bioelectron. 122 (2018) 16-24.

[41] A. Dalui, B. Pradhan, U. Thupakula, A.H. Khan, G.S. Kumar, T. Ghosh, B. Satpati, S. Acharya, Insight into the mechanism revealing the peroxidase mimetic catalytic activity of quaternary CuZnFeS nanocrystals: colorimetric biosensing of hydrogen peroxide and glucose, Nanoscale 7 (2015) 9062-9074.

[42] I. Fratoddi, Hydrophobic and hydrophilic Au and Ag nanoparticles. Breakthroughs and perspectives, Nanomaterials 8 (2018).

[43] W.J. Jin, J.M. Costa- Fernández, R. Pereiro, A. Sanz-Medel, Surface-modified CdSe quantum dots as luminescent probes for cyanide determination, Anal. Chim. Acta 522 (2004) 1–8.

[44] J.M. Costa- Fernández, R. Pereiro, A. Sanz-Medel, The use of luminescent quantum dots for optical sensing, Trac-Trend. Anal. Chem. 25 (2006) 207-218.

[45] J.B. Murray, H.I. Al-Shora, Stability of cocaine in aqueous solution, J. Clin. Pharm. Ther, 3 (1978) 1-6.

[46] V.D. Gupta, Stability of cocaine hydrochloride solutions at various pH values as determined by high-pressure liquid chromatography, Int. J. Pharmaceut. 10 (1982) 249-257.

[47] J. Shah, R. Purohit, R. Singh, A.S. Karakoti, S. Singh, ATP-enhanced peroxidase-like activity of gold nanoparticles, J. Colloid Interf. Sci. 456 (2015) 100–107.

[48] M.N. Stojanovic, P. de Prada, D.W. Landry, Aptamer-based folding fluorescent sensor for cocaine, J. Am. Chem. Soc. 123 (2001) 4928-4931.

[49] A.J. Johnston, S. Busch, L.C. Pardo, S.K. Callear, P.C. Biggin, S.E. McLain, On the atomic structure of cocaine in solution, Phys. Chem. Chem. Phys. 18 (2016) 991-999.

[50] V. Ladroue, L. Dujourdy, F. Besacier, P. Jame, IRMS to study a common cocaine cuttingagent: phenacetin, Drug. Test. Analysis 9 (2017) 479-484.

[51] J.D. Pope, O.H. Drummer, H.G. Schneider, The cocaine cutting agent levamisole is frequently detected in cocaine users, Pathology 50 (2018) 536-539.

[52] United Nations Office on Drugs and Crime, Recommended methods for the identification and analysis of cocaine in seized materials. 2012. https://www.unodc.org/documents/scientific/Cocaine_Manual_Rev_1.pdf

[53] Y. Du, B. Li, S. Guo, Z. Zhou, M. Zhou, E. Wang, S. Dong, G-Quadruplex-based DNAzyme for colorimetric detection of cocaine: Using magnetic nanoparticles as the separation and amplification element, Analyst, 136 (2011) 493–497.

[54] M.N. Stojanovic, D.W. Landry, Aptamer-based colorimetric probe for cocaine, J. Am. Chem. Soc. 124 (2002) 9678–9679.

[55] J. Nie, Y. Deng, Q.-P. Deng, D.-W. Zhang, Y.-L. Zhou, X.-X. Zhang, A self-assemble aptamer fragment/target complex based high-throughput colorimetric aptasensor using enzyme linked aptamer assay, Talanta 106 (2013) 309−314.

[56] J. Zhang, L. Wang, D. Pan, S. Song, F.Y.C. Boey, H. Zhang, C. Fan, Visual cocaine detection with gold nanoparticles and rationally engineered aptamer structures, Small 4 (2008) 1196–1200.

[57] J. Liu, Y. Lu, Fast colorimetric sensing of adenosine and cocaine based on a general sensor design involving aptamers and nanoparticles, Angew. Chem. Int. Ed. 45 (2005) 90–94.

Table 1. Comparison of the analytical performance of the CTAB-AuNP-$_{L}$-cyst-ZnSeS QDs hybrid nanozyme peroxidase-like catalytic cocaine colorimetric biosensor with other published colorimetric biosensors for cocaine.

Strategy	Method	LOD	Detection time	Ref.
Magnetic NP-aptamer G-quadruplex-based DNAzyme-hemin	Colorimetry	0.05 μM	20 min	**[53]**
Aptamer organic dye-displacement	Colorimetry	500 μM	12 hours	**[54]**
Enzyme linked aptamer assay	Colorimetry	2.8 μM	60 min	**[55]**
Split aptamer ligation-AuNPs	Colorimetry	2 μM	10 min	**[56]**
Thiol-DNA aptamer-aggregated AuNPs	Colorimetry	1000 μM	12 hours	**[57]**
58 nm CTAB-AuNP-$_{L}$-cyst-ZnSeS QDs hybrid nanozyme	Colorimetry	0.128 μM	2 min	This work

Table 2. Analytical performance of the CTAB-AuNP-$_{L}$-cyst-ZnSeS QDs hybrid nanozyme peroxidase-like catalytic sensor for cocaine detection in mixed drug samples. All data recorded at ~2 min.

Mixed drug (100 µM)	**Cocaine added (µM)**	**Found (µM)**	**Recovery (%) ±SD (%)**	**RSD (%)**
Phenacetin	100	93.2	93.2±7.2	8.1
	75	74.8	99.8±4.4	5.4
	50	50.3	100.6±1.5	3.0
Diltiazem	100	86.7	86.7±6.7	8.4
	75	71.5	95.3±4.8	6.0
	50	54.0	108.0±0.4	0.7
Levamisole	100	82.2	82.2±8.9	12.1
	75	66.1	86.6±2.3	3.0
	50	48.5	97.0±1.6	3.2

SD = Standard deviation of three replicate measurements.

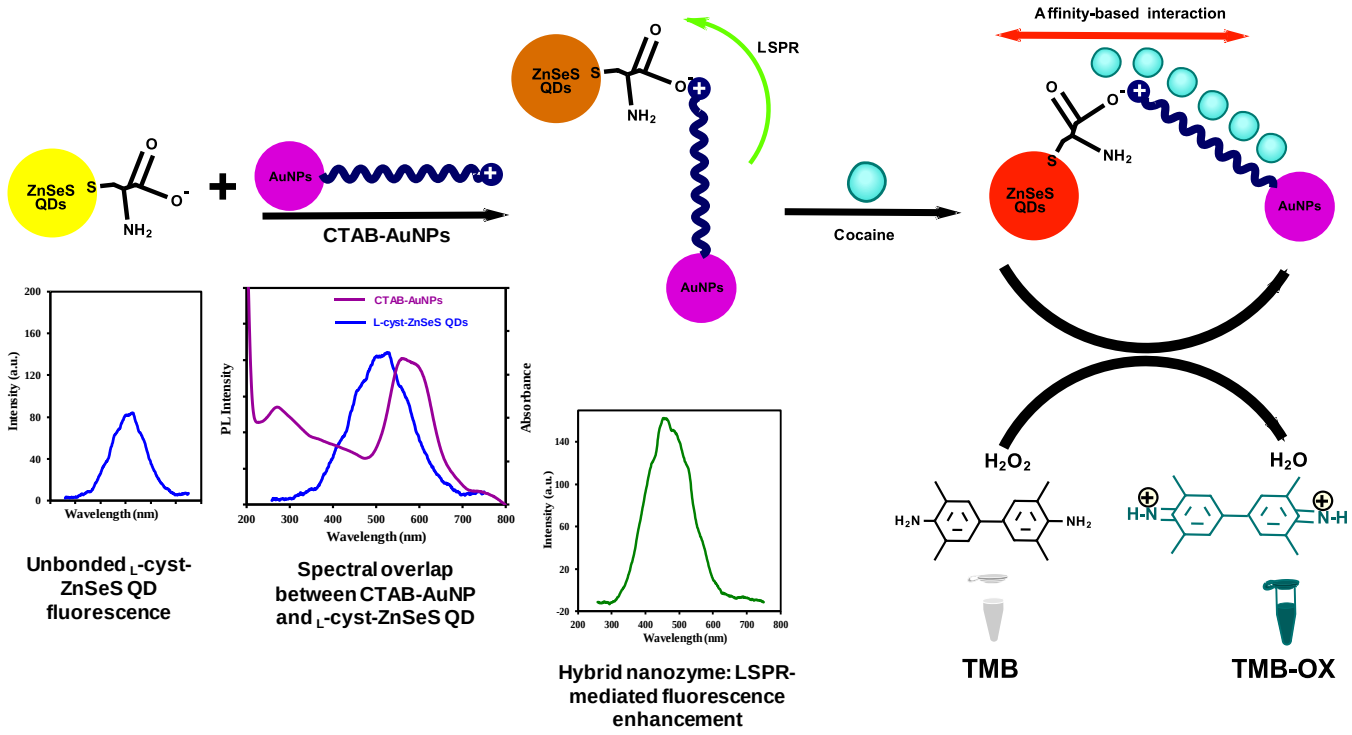

Scheme 1. Schematic description of the CTAB-AuNP-$_{L}$-cyst-ZnSeS QDs hybrid nanozyme peroxidase-like catalytic sensor for cocaine.

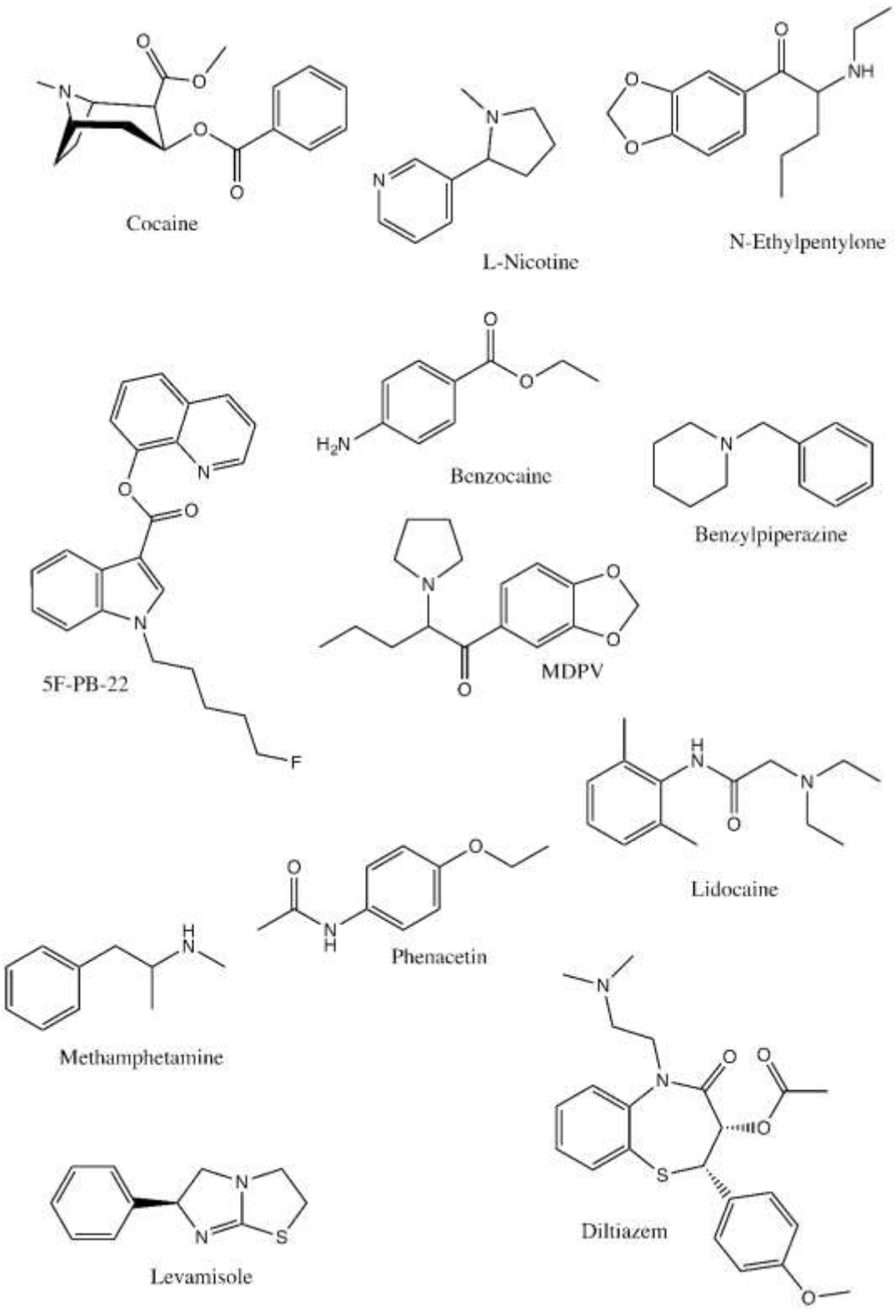

Scheme 2. Structure of cocaine and other drug compounds used as tested interferents in the developed peroxidase-like catalytic assay.

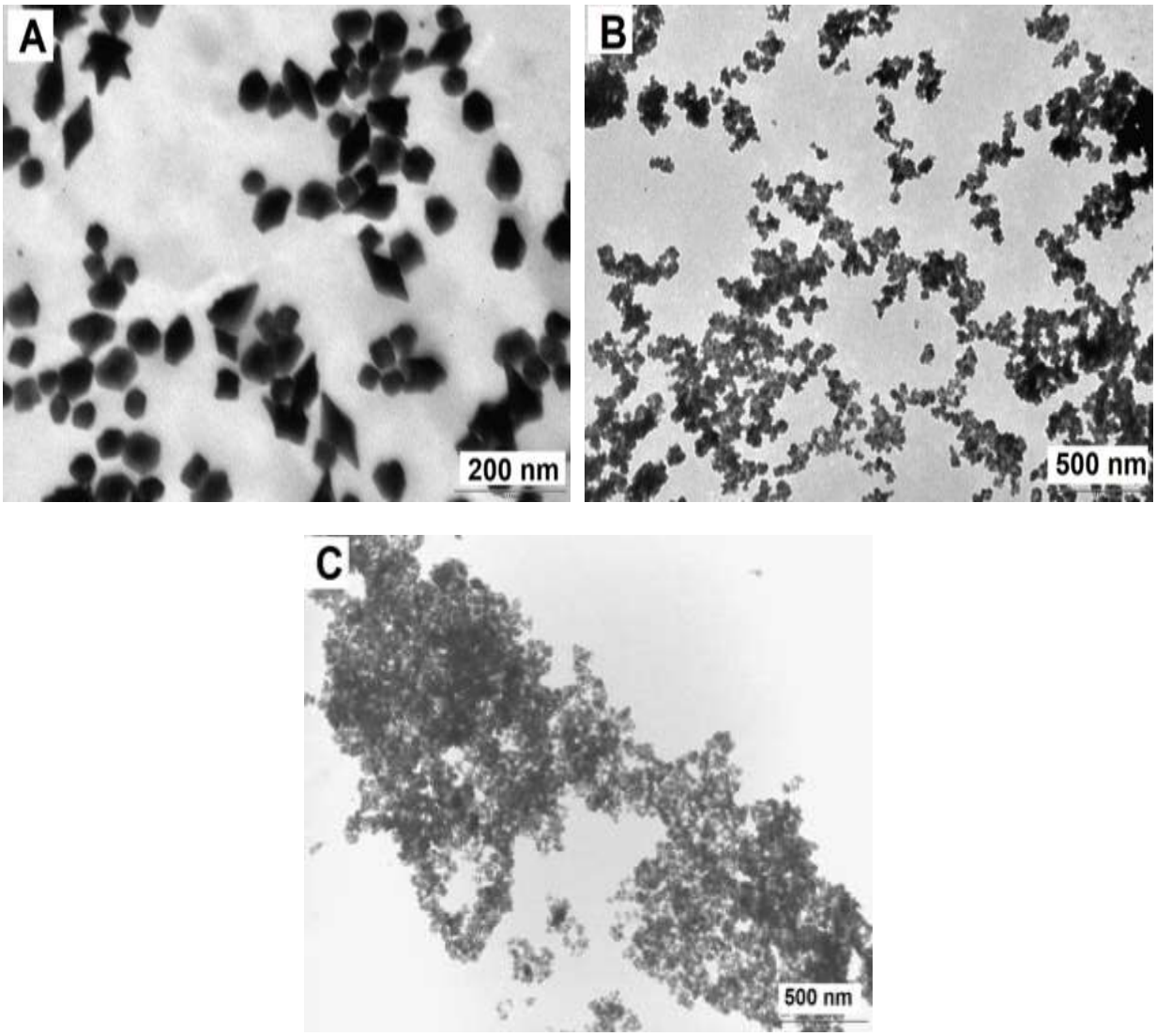

Fig. 1. TEM images of (A) multi-shaped CTAB-AuNPs, (B) $_{L}$-cyst-ZnSeS alloyed QDs and the (C) hybrid QDs-CTAB-AuNP-nanozyme.

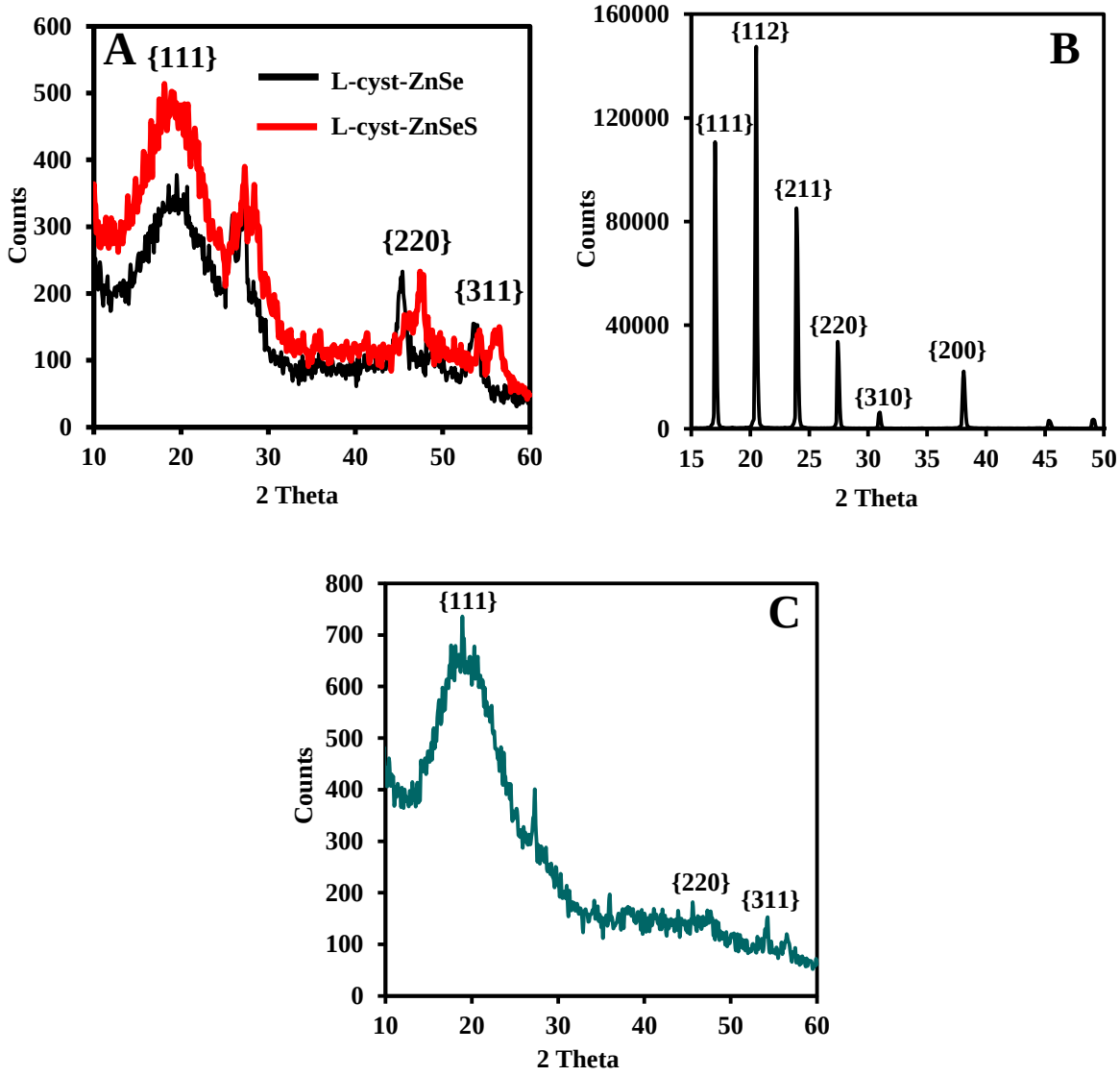

Fig. 2. PXRD pattern of (A) $_{L}$-cyst-ZnSe core and $_{L}$-cyst-ZnSeS alloyed QDs, (B) CTAB-AuNPs and the (C) hybrid QDs-CTAB-AuNP nanozyme.

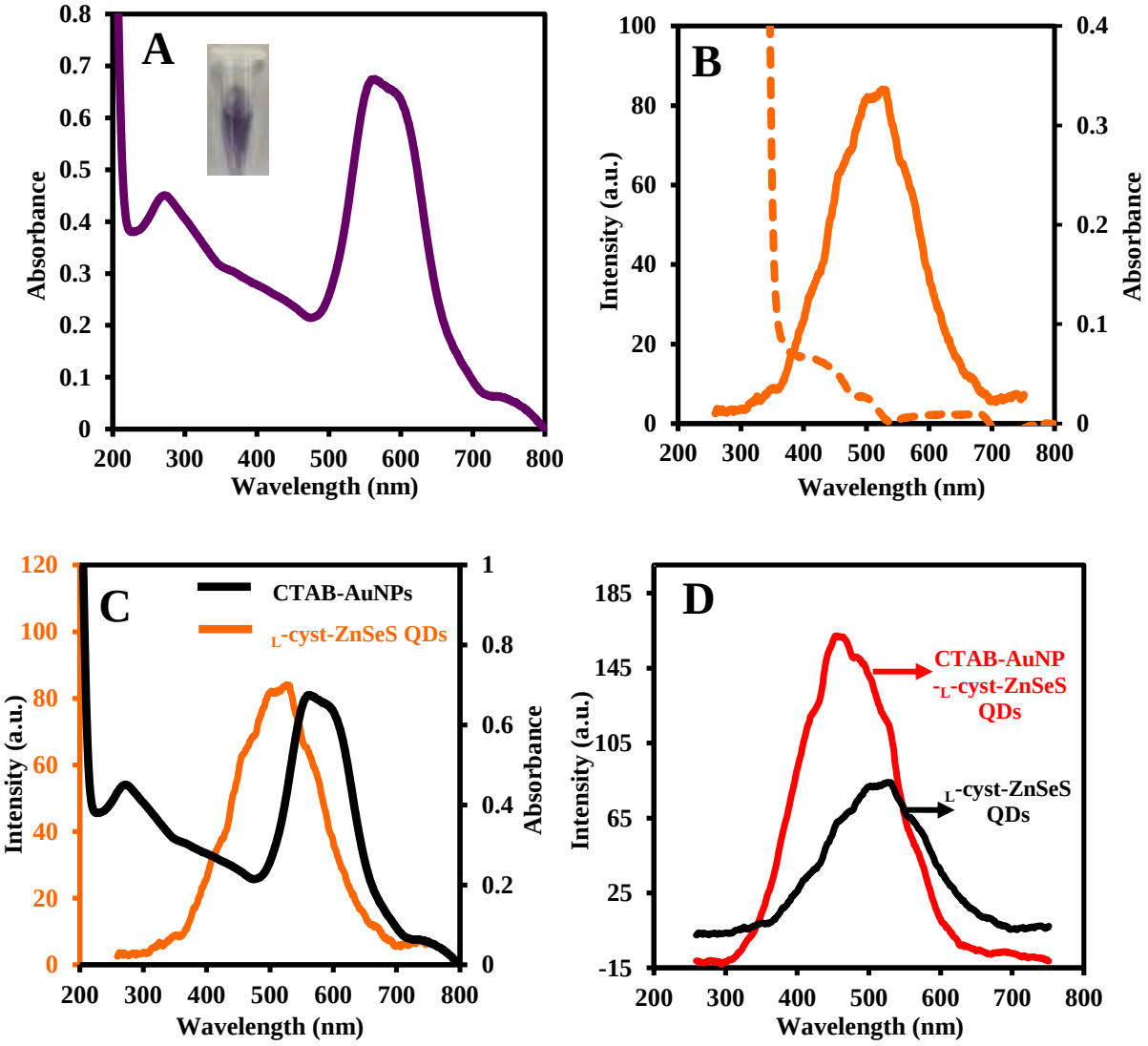
A
Absorbance
Wavelength (nm)
B
Intensity (a.u.)
Absorbance
Wavelength (nm)
C
CTAB-AuNPs
L-cyst-ZnSeS QDs
Intensity (a.u.)
Absorbance
Wavelength (nm)
D
CTAB-AuNP
-L-cyst-ZnSeS
QDs
L-cyst-ZnSeS
QDs
Intensity (a.u.)
Wavelength (nm)

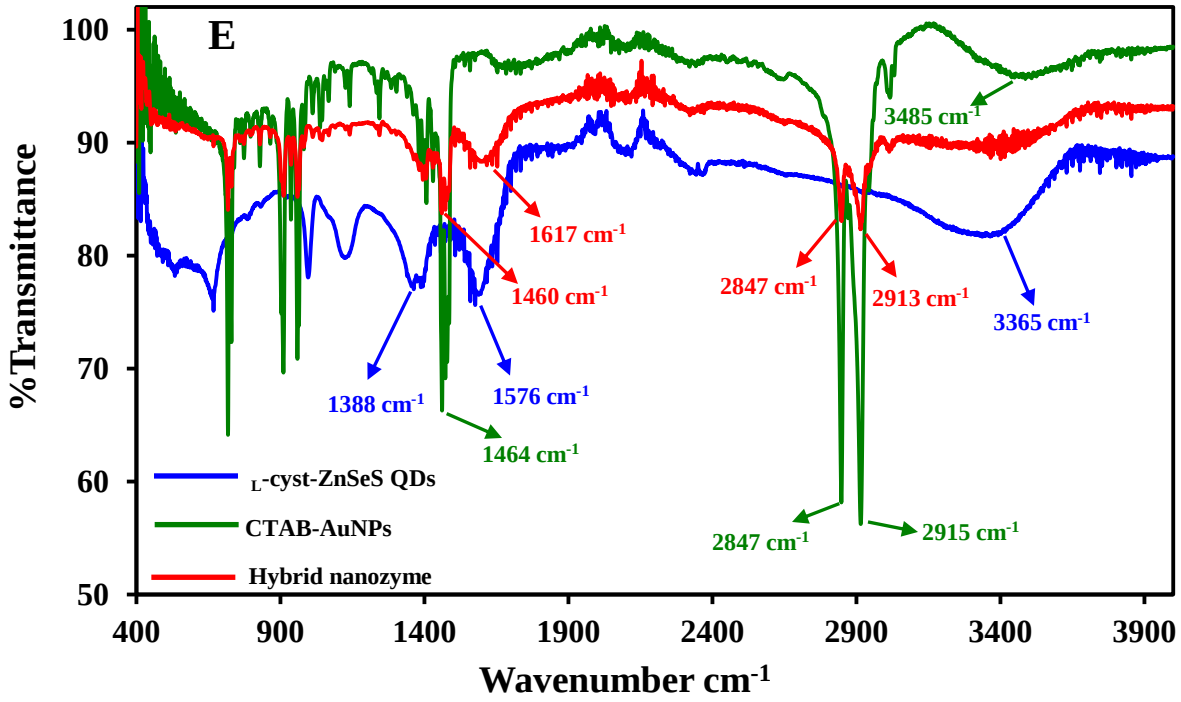

Fig. 3. (A) UV/vis absorption spectrum of multi-shaped CTAB-AuNPs Inset: Photograph of the multi-shaped CTAB-AuNPs in solution., (B) UV/vis absorption (dotted line) and fluorescence emission spectra (solid line) of $_{L}$-cyst-ZnSeS alloyed QDs, (C) spectral overlap between CTAB-AuNPs and $_{L}$-cyst-ZnSeS QDs, (D) LSPR-induced fluorescence enhancement of CTAB-AuNPs-$_{L}$-cyst-ZnSeS QDs and (E) FT-IR spectra of the QDs, CTAB-AuNPs and the hybrid QDs-CTAB-AuNP nanozyme.

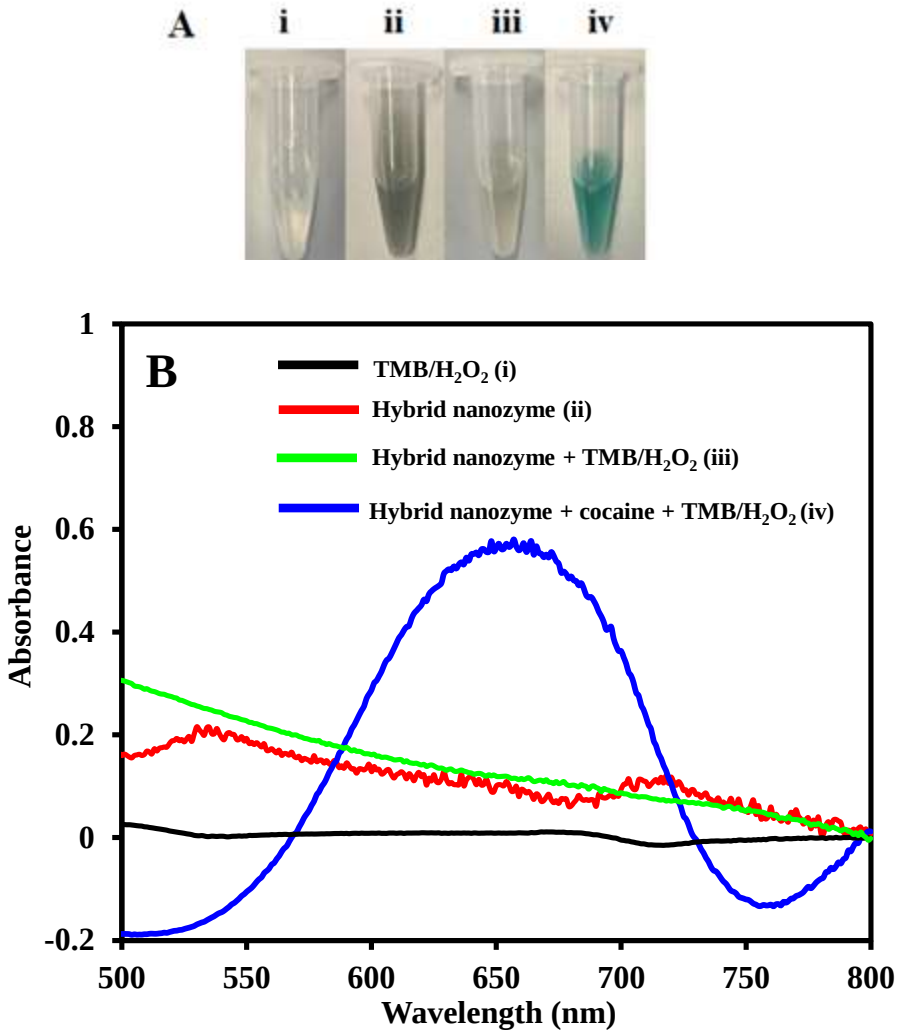

Fig. 4. (A) Photograph of (i) TMB/H_2O_2, (ii) hybrid nanozyme, (iii) hybrid nanozyme + TMB/H_2O_2 and (iv) hybrid nanozyme + cocaine + TMB/H_2O_2. (B) Corresponding UV/vis absorption spectra of (i), (ii), (iii) and (iv). [Cocaine] = 100 µM. Reaction carried out at room temperature.

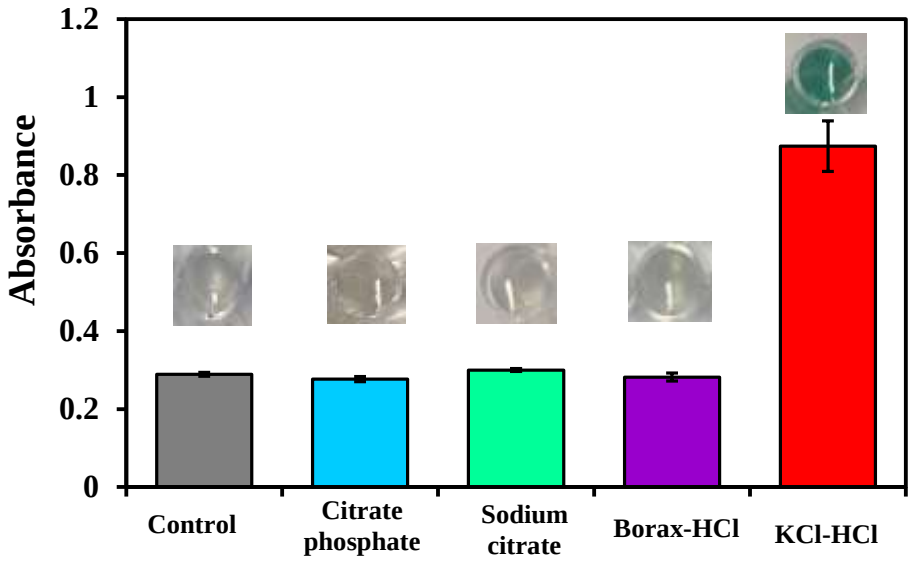

Fig. 5. Catalytic response of the QDs-CTAB-AuNP hybrid nanozyme to cocaine (100 µM) in different buffer solution. Inset: Photographic colour of the QDs-CTAB-AuNP hybrid nanozyme to cocaine detection in the different buffer solution. Hybrid nanozyme (CTAB-AuNPs (0.02 nM) + $_{L}$-cyst-ZnSeS alloyed QDs (3 mg/mL); TMB (0.003 M); H_2O_2 (1.2 M); Data recorded at ~2 min. Reaction carried out at room temperature. Error bars represents standard deviation of three replicate analysis.

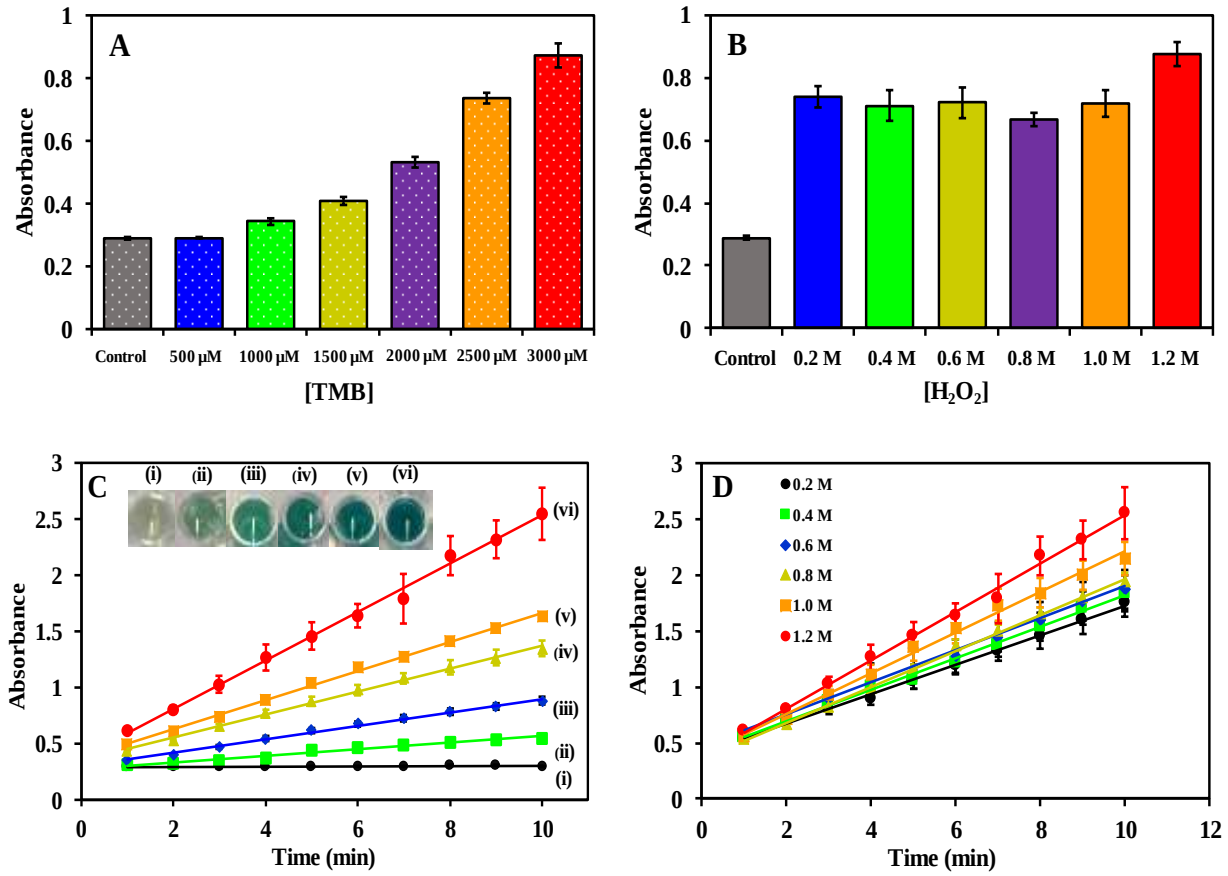

Fig. 6. Catalytic response of the hybrid QDs-CTAB-AuNP nanozyme to cocaine (100 µM) detection as it relates to the effects of different (A) TMB concentration (fixed H_2O_2 concentration = 1.2 M) and (B) H_2O_2 concentration (fixed TMB concentration = 3000 µM). Time course kinetic effects of varying TMB concentration (H_2O_2 fixed) (C) and H_2O_2 concentration (TMB fixed) (D) on the catalytic peroxidase activity of the hybrid nanozyme to cocaine detection. Fig. 3C: (i) 500 µM, (ii) 1000 µM, (iii) 1500 µM, (iv) 2000 µM, (v) 2500 µM and (vi) 3000 µM. Inset of Fig. 3C: Photographic colour of the hybrid nanozyme to cocaine detection taken at the end of the time-course assay as it relates to different TMB concentration. Control = nanozyme solution + KCl-HCl, pH 2.2 buffer (no cocaine). Reaction carried out at room temperature. Error bars represents standard deviation of three replicate analysis.

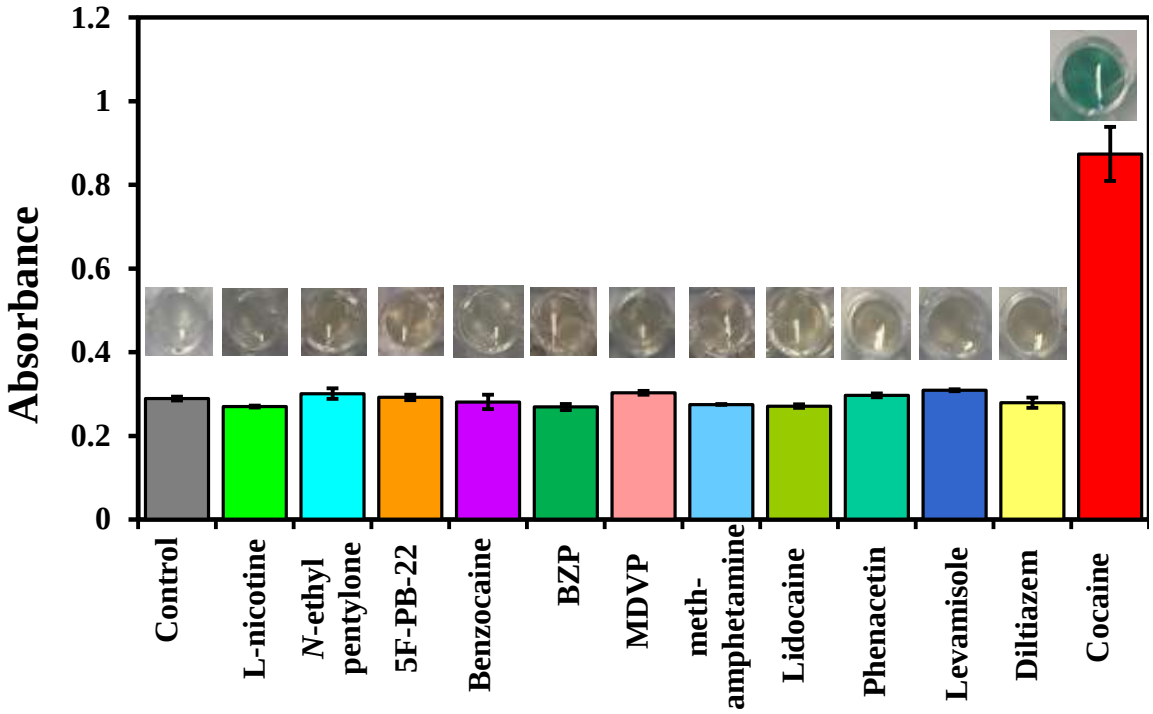

Fig. 7. Selectivity of the QDs-CTAB-AuNP hybrid nanozyme biosensor to cocaine in comparison to other drug targets. Concentration of cocaine and other targets = 100 µM in 0.1 M KCl-HCl, pH 2.2 buffer. Hybrid nanozyme (CTAB-AuNPs (0.02 nM) + $_{L}$-cyst-ZnSeS alloyed QDs (3 mg/mL); TMB (0.003 M); H_2O_2 (1.2 M); Data recorded at ~2 min. Reaction carried out at room temperature. Error bars represents standard deviation of three replicate analysis.

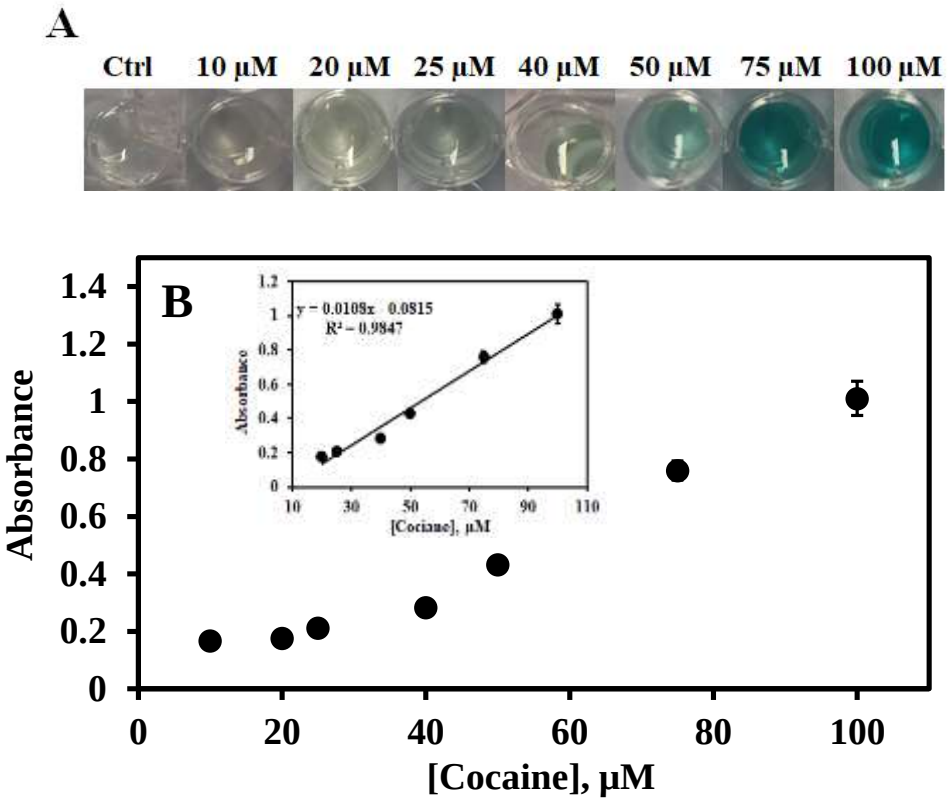

Fig. 8. (A) Photographic display of the colorimetric response of the QDs-CTAB-AuNP hybrid nanozyme for the detection of each cocaine concentration after adding TMB-H_2O_2 and (B) Quantitative calibration signal plot for cocaine detection. Hybrid nanozyme (CTAB-AuNPs (0.02 nM) + $_L$-cyst-ZnSeS alloyed QDs (3 mg/mL); TMB (0.003 M); H_2O_2 (1.2 M); Data recorded at ~2 min. Inset: Linear calibration plot. Error bars represents standard deviation of three replicate analysis.